1 **Optimization of Electrocatalyst Performance of Platinum-Ruthenium induced with**

2 **MXene by Response Surface Methodology for Clean Energy Application**

3

4 Norulsamani Abdullah[1], Rahman Saidur[1,2,*], Azran Mohd Zainoodin[3], Navid Aslfattahi[4]

5
6 [1]*Research Center for Nano-Materials and Energy Technology (RCNMET), School of Science and Technology,*
7 *Sunway University, Bandar Sunway, Petaling Jaya, 47500, Selangor Darul Ehsan, Malaysia*
8 [2] *Department of Engineering, Lancaster University, Lancaster, LA1 4YW, UK*
9 [3] *Fuel Cell Institute, Universiti Kebangsaan Malaysia, 43600 UKM Bangi, Selangor, Malaysia*
10 [4]*Department of Mechanical Engineering, Faculty of Engineering, University of Malaya, 50603, Kuala Lumpur,*
11 *Malaysia*
12
13 Corresponding authors: saidur@sunway.edu.my
14

15 **ABSTRACT**

16 Fuel cell produces clean sources of energy and yielding can be improved using emerging

17 material, MXene, in electrocatalysis performance in fuel cell system. However, MXene in

18 electrocatalysis area for fuel cell is not discovered yet. Therefore, the aim of this study is to

19 enhance the direct methanol fuel cell (DMFC) electrocatalyst performance using combination

20 of bimetallic, PtRu, and MXene. Optimization is carried out using response surface

21 methodology (RSM). Composition of MXene, Nafion content and methanol concentration are

22 used as factors (input) and current density response is used as response (output) for the

23 optimization analysis. Cyclic voltammetry (CV) is used to measure current density. RSM

24 generates optimum factors with MXene composition 78.90wt%, Nafion content 19.71wt% and

25 methanol concentration of 2.82M. The optimum response is predicted to be 186.59mA/mg$_{PtRu}$.

26 The validation test is carried out and the result shows that the average current density is

27 187.05mA/mg$_{PtRu}$. The comparison of current density at the same condition show that

28 PtRu/MXene electrocatalyst have 2.34 times higher compared with PtRu/C commercial

29 electrocatalyst and this indicates that MXene has high potential as a nanocatalyst for cleaner

30 energy production through fuel cell.

1. **INTRODUCTION**

MXene is an emerging layered material attracted tremendous interest by scientific community since it's invention by Drexel University researchers in 2011. This is due to it's unique mechanical and electronic properties large surface areas (Khazaei et al., 2019). There are at least 18 types of nanomaterials that are listed in this group. The materials are graphene, MXenes, graphitic carbon nitride (g-C_3N_4), hexagonal boron nitride (h-BN), black phosphorus (BP), transition metal oxyhalides, metal oxides, metal halides, metals and others (Zhu et al., 2017). MXene can be obtained by eliminating element A from a ternary parent MAX phases (with general formula of $M_{n+1}AX_n$). MXene consist of nitrides, transition metal carbides and carbonitrides (Kuang et al., 2019). Up to now, more than 70 MAX phases have been reported worldwide. However, only 9 MXenes are established like Ti_2C, Ti_3C_2, Ti_3CN, $(Ti_{0.5}, Nb_{0.5})_2C$, V_2C, $(V_{0.5}, Cr_{0.5})_3C_2$, Ta_4C_3, Nb_4C_3 and Nb_2C are produced out of 70 MAX phases (Lei et al, 2015).

MXene is a promising candidate for diverse applications, especially for electronic (Khazaei et al., 2019), energy storage and electrochemical biosensors (Lei et al, 2015). Besides that, this material is also has great potential in electrocatalysis for hydrogen oxidation reaction (HOR), oxygen reduction reaction (ORR), hydrogen evolution reaction (HER), oxygen evolution reaction (OER), carbon dioxide reduction reaction (CO_2RR) (Chia and Pumera, 2018; Xia et al., 2019), and methanol oxidation reaction (MOR) (Wang et al., 2019). The implementation of MXene as one of the electrocatalyst component has been investigated by few researchers. Zhang et al. (2016) synthesized the new MXene/Ag composites and found that the composites exhibited the electrocatalytic activity for ORR with 3.31mA/cm^2 of current

density due to the shortening diffusion path of adsorbed oxygen and numerous oxygen adsorption sites. Wang et al. (2019) enhanced the MOR with Pt decorated Ti_3C_2 MXene and reported three times higher performance compared to a commercial electrocatalyst. Tran et al. (2018) successfully developed V_4C_3Tx MXene for the electrocatalytic activity of HER. All these reactions are important for the clean energy applications. One of the promising clean energy productions that gain a research interest is direct methanol fuel cell (DMFC).
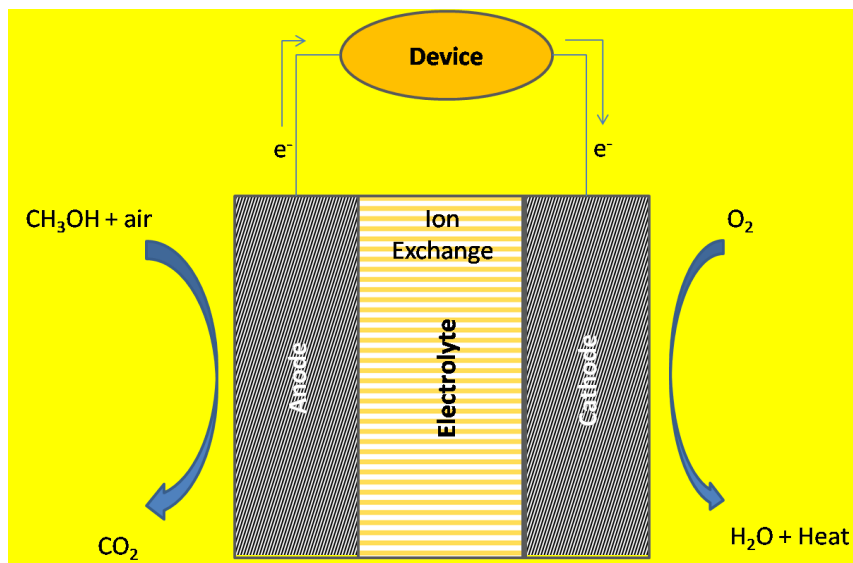
Fig. 1. The illustration of DMFC system.

The DMFC, also known as the leading direct liquid fuel polymer electrolyte membrane fuel cells (PEMFC), produces clean energy directly from high energy density liquid methanol fuel (Joghee et al., 2015). The full schematic diagram for DMFC system is shown in Fig. 1. DMFCs play a vital role in clean energy production..Li-ion batteries faced challenges like low energy density, loss of 35% of energy capacity within 24 months, self-discharging and capacity face issues (Stone 2007). DMFCs might overcome these challenges. Higher energy density of methanol fuel cell (15 times higher than the energy density of a Li-ion battery) provides an opportunity for DMFCS to be considered as a potential area for clean energy production. However, this technology still has issues such as catalyst poisoning and slow reaction of

electrochemical reaction. These problems lead to increasing activation anode potential, reduce cell voltage and efficiency. These consequently, reduce the system performance and power output (Karim and Yahya, 2018; Abdullah et al., 2017). The MOR and ORR is the main reactions occur for anode and cathode side in DMFC.

Lin et al. (2019) successfully fabricated free-standing ultrathin two-dimensional (2D) MXene nanosheets. The fabricated MXene with extremely small thickness and provided desirable stability and activity in alkaline media that leads to the high ORR performance. Xie et al. (2013) also reported ORR using platinum (Pt) nanoparticles supported on 2D MXene nanosheets. The catalyst showed a superior performance due to the unique properties of MXene like strong anchorage to Pt nanoparticles, high corrosion resistance and good conductivity that make it ideal as a catalyst. Yang et al. (2019) used Ti_3C_2Tx MXene nanosheets decorated on multiwall carbon nanotubes (MWCNTs) with molybdenum disulfide (MoS_2) quantum dots and showed remarkable electrocatalytic performances for ORR and MOR in an alkaline solution. Zhang et al. (2019) later reported Pt-based electrocatalysts that consist of 2D Ti_3C_2Tx nanosheets connected by one-dimensional (1D) MWCNTs for MOR. They reported that the well dispersion of Pt nanoparticles on MXene nanosheet help to boost high electrochemical active surface area (ECSA) that lead to the outstanding electrochemical performance. However, the optimum value for the main parameter and the bimetallic catalyst of Pt and ruthenium (Ru) induced with MXene as an electrocatalyst for MOR is not reported yet. New optimized model was developed using response surface methodology (RSM). New MXene based catalyst with PtRu is formulated for the first time. A current density, 187.05mA/mg_{PtRu}, which is 2.34 higher than PtRu/C (79.32mA/mg_{PtRu}.) is found higher than available literatures. These are the novel parts of the current research compared to available literatures.

The optimization can be defined as a process of determining the optimum solutions to certain mathematically defined problems (Fletcher, 2013). RSM is the most satisfying

98   optimization method used by researchers lately in various fields of research (Asfaram et al,

99   2015; Dharma et al., 2016; Danmaliki et al., 2017; Sulaiman et al., 2018; Caponi et al., 2019).

100 This method involves a collection of mathematical and statistical techniques that are useful for

101 improving, developing and optimizing processes (Myers et al., 2016). RSM can determine the

102 effects of independent variables either individually or in combination of a process and able to

103 reduce the number of experiments needed to analyze the process statistically by a variety of

104 factors (Khatti et al.; 2017). The effectiveness of this optimization method in a fuel cell is also

105 reported in the literatures (Yahya et al., 2017; Abdullah et al., 2019; Shaari et al., 2018).

106   The defined problem in this study is the 'best' value of factors that relatively can affect

107 the electrocatalytic activity for methanol oxidation. The factors are composition of MXene,

108 Nafion content, and methanol concentration. All these factors are agreed as the most affected

109 factors for DMFC application (Ito et al., 2013; Zainoodin et al., 2015; Vecchio et al., 2018).

110 The MXene composition is a crucial factor for this model since the MXene acts as a catalyst

111 support for this electrocatalyst and the changes in the amount of material can give the high

112 impact to the reaction itself (Abdullah et al., 2019). Besides, nafion ionomer acts as a physical

113 binder for the particles of catalyst support, which assist to retain moisture in the electrode

114 surface area and helps to extend the three-phase boundary. However, excessive use of Nafion

115 can lead to an increase in the mass transfer resistance (Adilbish and Yu, 2017) and too low

116 Nafion content results in poor cell performance due to poor bonding between the particles of

117 electrocatalyst and the electrolyte (Masdar et al., 2016). High concentration of methanol helps

118 in the production of high energy densities and thus enhances cell performance (Vecchio et al,

119 2018) but too high in concentration also can decrease the active sites on the electrode (Kivrak,

120 2015).

121   The bimetallic catalyst PtRu integrated with 2D structure of MXene is the first time

122 formulated for the DMFC application. Hence, this paper is focusing on the optimization and

improvement of the MXene incorporated electrocatalyst performance for MOR by using RSM approach. The factors involved for the RSM method are composition of MXene, methanol concentration and Nafion loading as well as current density as a response for electrocatalytic activity in DMFC performance. The MXene was prepared using etching method and the PtRu was deposited onto the MXene nanoparticle. The synthesized PtRu/MXene electrocatalyst has undergone scanning electron microscope (SEM) for the physical characterization. The RSM optimization with three factors and one response was run via design of experiment for electrochemical testing was evaluated by a cyclic voltammetry (CV). The developed RSM shows a fit model and provide a significant result that can be used to be further analysed in the design space. This paper also provides better MOR performance compared with other commercial DMFC electrocatalyst due to the strong bonding between PtRu and MXene and unique structure of 2D material that can provide a large active site on the surface of electrocatalyst.

2. EXPERIMENTAL

2.1. Materials and Chemicals

Pt Precursor, H_2PtCl_6 (37.5% content), Ru Precursor, Ru_3Cl (45-55% content) and sodium borohydride, $NaBH_4$ (99%) were received from Sigma Aldrich, Germany. Meanwhile, isopropyl alcohol (IPA, 99.8%) and nafion solution D520 (5wt%) were obtained from Chemiz, Malaysia and Chemours.com, respectively.

2.2. Preparation of PtRu/MXene Electrocatalyst

MXene was synthesized using the etching method with ammonium hydrogen difluoride (NH_4HF_4) as an etching agent by Aslfattahi et al. (2020). Meanwhile, all the electrocatalysts were prepared by depositing the Pt and Ru onto the MXene using chemical reduction method. The Pt and Ru were loaded using the precursor with the atomic ratio 1:1. The MXene was

added in the deionized water (DI water) and IPA mixture with the 1:1 volume ratio and sonicated for 30min. Then, the Pt and Ru precursor were added into a mixture and stirred continuously for 30min or until homogenous at ambient temperature. The pH value of the mixture is altered to 8 using 1M of sodium hydroxide (NaOH) solution and increased the temperature to $80^{o}C$. After that, 25mL of 0.2M reducing agent, $NaBH_4$, was added into the mixture and stirred continuously for an hour. The mixture is cooled and centrifuged for 15min at 15,000 rpm. The sediment was washed and centrifuged repeatedly using DI water. The collected sediment was dried for 3h at $120^{o}C$ under a vacuum condition. The dried sediment, also called as an electrocatalyst was crushed using a set of pestle and mortar. This procedure was repeated for different composition of MXene. The electrocatalyst sample is ready to be used for the physical characterization and electrochemical measurement.

2.3.   Surface morphology of PtRu/MXene Electrocatalyst

The surface morphology of electrocatalyst was analyzed using SEM, TESCAN VEGA3, France. Besides, the energy-dispersive X-ray (EDX) and mapping using AZtec analysis software, Oxford Instrument, France, also were conducted to analyse the elemental composition and distribution of the electrocatalyst sample.

2.4.   Electrochemical Measurement

The electrocatalyst performance for the PtRu/MXene electrocatalyst was measured through CV test by using an electrochemical workstation (Interface 1010E, Gamry Instruments, USA). The CV was evaluated using three-electrode cell system, that consists of glassy carbon electrode (GCE, 3mm-inner diameter), Pt electrode and silver/silver chloride electrode (Ag/AgCl); as working, counter and reference electrode. All the electrodes were purchased from Metrohm, Switzerland. The working electrode need some preparation before available

173   for the testing. The GCE was cleaned by using a polished paper and alumina to ensure that no

174   unnecessary element cover the surface of an electrode. Next, the electrocatalyst ink was

175   prepared, where 12.5mg of electrocatalyst was added into 100µL of nafion solution, 300µL of

176   DI water and 300µL of IPA. The electrocatalyst mixture was dispersed using an ultrasonic

177   crusher for 90s or until homogenous. Then, 2.5µL of electrocatalyst ink was pippeted onto the

178   GCE surface and left for 1h at ambient condition before further dried for another 30min at

179   80ºC. The procedure is repeated using different composition of MXene and Nafion loading.

180   The GCE electrode was ready for further used in CV test. The electrolyte of 0.5M sulphuric

181   acid (H_2SO_4) in 2M methanol was prepared for the CV measurement. The concentration of the

182   methanol was changed based on the schedule from design of experiment. The nitrogen gas was

183   bubbled into electrolyte for 20min to produce saturated nitrogen condition. This measurement

184   was performed within -0.2 to 1.0 V vs. Ag/AgCl potential range at 20mV/s scan rate in room

185   temperature.

186

187   **2.5. Experimental Design**

188   The impact of factors towards certain response was estimated using central composite design

189   (CCD), that consists of three parts, which is full factorial design, additional design and a central

190   point (Bezerra et al., 2008). Composition of MXene, nafion content and methanol

191   concentration were chosen as factors while current density that measured from electrochemical

192   measurement was chosen as a response. This experimental design was performed by using

193   Design Expert 8.0.7.1 (Stat-Ease Inc., Minneapolis, USA). All factors chosen were studied in

194   five different levels (-α, -1, 0, +1, +α). From the three factors and one response, the CCD

195   generated 20 experiments. The experimental data were matched with the second-order

196   polynomial regression model as presented in the equation (1), where y represents the predicted

197   response variable, k is the number of variables and β_0 is the constant term, $\beta_i, \beta_{ii}, \beta_{ij}$ are the

198   coefficients of the linear, quadratic and interaction parameters, x_i is the variables and ε is the

199   residual associated to the experiments (Bezerra et al., 2008):

200    $$y = \beta_0 + \sum_{i=1}^{k} \beta_i x_i + \sum_{i=1}^{k} \beta_{ii} x_i^2 + \sum_{1 \leq i \leq j}^{k} \beta_{ij} x_i x_j + \varepsilon \qquad (1)$$

201   The developed model was studied by analysing the coefficient of regression, analysis of

202   variance (ANOVA) and diagnostic of the model graphs. Besides that, the fit quality of the

203   equation model was measured by the coefficient of determination, R^2.

204

205   **3.   RESULTS AND DISCUSSION**

206   **3.1. Surface morphology of PtRu/MXene Electrocatalyst**

207   Surface morphology of electrocatalyst was analyzed by SEM to see the external morphology

208   of the electrocatalyst, distribution of bimetallic Pt and Ru on top of the MXene structure as

209   well as elemental mapping. These functions can be one of the indicators to exhibit the good

210   catalytic activity during the CV electrochemical testing. The morphology of the MXene and

211   electrocatalyst are shown in Fig. 2. SEM image for MXene and PtRu/MXene are captured at

212   magnification of 22kX and 5kX, respectively. The SEM image of MXene illustrates that the

213   2D MXene structure is successfully created, where the MXene structure resembling a 'sheet of

214   a wet book' can be seen prominently in the diagram. Fig. 2(b) is the SEM image of the

215   PtRu/MXene electrocatalyst, and it is noticeable that there are small particles dispersed and

216   covered the 2D MXene structure.
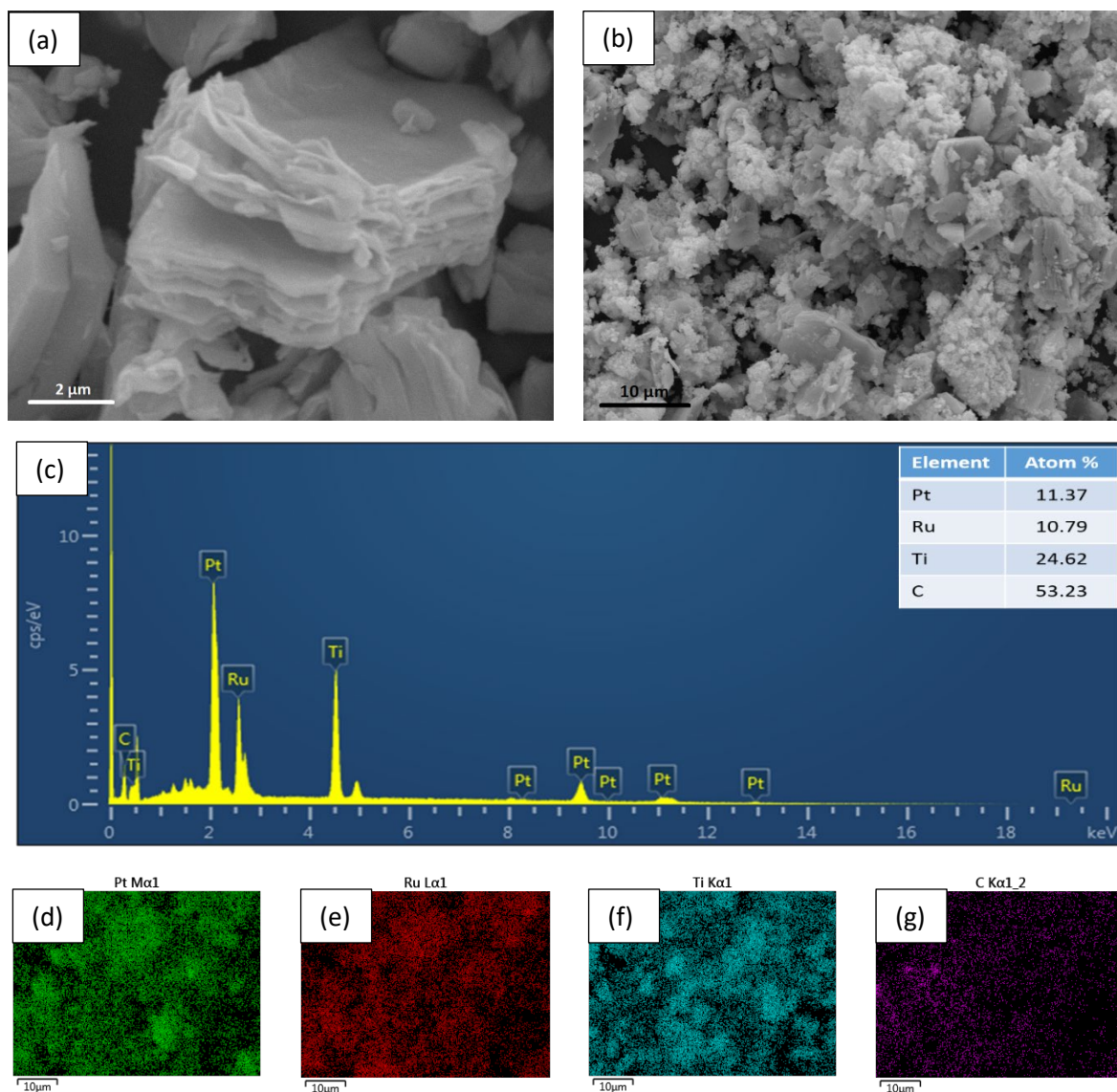
Fig. 2. Surface morphology for (a) SEM of MXene, (b) SEM of PtRu/MXene, (c) EDX analysis of PtRu/MXene, and (d) – (g) Mapping analysis for PtRu/MXene

To further identify the particles presence in MXene, EDX and mapping analysis are performed and shown in the Fig. 2(c) – (g). The results show the presence of four elements in the electrocatalyst, namely Pt, Ru, Ti and C. All of these elements are the major elements that must exist in the electrocatalyst and there is no impurity presence in the sample. Electrocatalyst mapping analysis exposed that the Pt and Ru particles are well distributed on the MXene structure. This will help in the creation of active response areas during catalytic activity and thus positively affect MOR. However, there are some agglomerations of Pt and Ru existed on

226 the sample due to the effect of NaOH overuse during pH adjustment in deposition process

227 (Deivaraj et al., 2005).

228

3.2. Optimization using RSM

230 The enhancement of the anodic electrocatalyst performance via optimization process using

231 RSM with CCD technique is carried out and involved three factors (composition of MXene,

232 Nafion content, methanol concentration) with one response (current density). MXene

233 composition is maintained in between 70 – 85wt%, nafion content is maintained in between 10

234 – 40wt% and methanol content is maintained in between 1 – 4M. These are chosen based on

235 the literature review (Zhang et al., 2019; Wang et al., 2019; Luo et al., 2019; Abdullah et al.,

236 2018; Zhang et al., 2018; Han et al., 2018; Adilbish and Yu, 2017; Park and Choi, 2017; Masdar

237 et al., 2016; Zainoodin et al., 2015) and one-factor-at-one-time experimental method. The

238 current density is chosen as a response because it is one of the most potential values for

239 electrocatalytic activity and performance for methanol oxidation reaction. All the experimental

240 factors and response are presented in Table 1. The quadratic model is developed and new

241 equation for the response is modelled by Eq. (2):

242 $Y=182.13+5.01A-17.44B+8.55C-14.84A^2-24.61B^2-19.45C^2-0.64AB+1.25AC+1.04BC$ (2)

243 Where, Y is the current density (mA/mg$_{PtRu}$), A is the composition of MXene (wt%), B is the

244 Nafion content (wt%) and C is the methanol concentration (M).

245

246

247 **Table 1** The CCD uncoded and coded (in bracket) of independent variables with

248 predicted and actual value of response for all runs

Run	Factor A	Factor B	Factor C	Response 1	
				Predicted Value	Actual Value
1	70.00 (-1)	10.00 (-1)	1.00 (-1)	128.75	135.16
2	70.00 (-1)	10.00 (-1)	4.00 (1)	141.26	140.06
3	85.00 (1)	40.00 (1)	1.00 (-1)	99.31	100.20
4	77.50 (0)	25.00 (0)	2.50 (0)	182.13	196.63
5	77.50 (0)	25.00 (0)	2.50 (0)	182.13	178.57
6	77.50 (0)	50.23 (1.682)	2.50 (0)	83.19	80.84
7	70.00 (-1)	40.00 (1)	1.00 (-1)	93.08	102.28
8	70.00 (-1)	40.00 (1)	4.00 (1)	109.75	110.08
9	77.50 (0)	25.00 (0)	2.50 (0)	182.13	180.13
10	77.50 (0)	25.00 (0)	-0.02 (-1.682)	112.73	103.16
11	77.50 (0)	-0.23 (-1.682)	2.50 (0)	141.84	144.64
12	77.50 (0)	25.00 (0)	2.50 (0)	182.13	176.80
13	77.50 (0)	25.00 (0)	2.50 (0)	182.13	179.53
14	77.50 (0)	25.00 (0)	5.02 (1.682)	141.49	151.51
15	64.89 (-1.682)	25.00 (0)	2.50 (0)	131.72	122.80
16	85.00 (1)	10.00 (-1)	1.00 (-1)	137.55	136.90
17	77.50 (0)	25.00 (0)	2.50 (0)	182.13	181.02
18	85.00 (1)	40.00 (1)	4.00 (1)	120.99	114.26
19	90.11 (1.682)	25.00 (0)	2.50 (0)	148.75	157.94
20	85.00 (1)	10.00 (-1)	4.00 (1)	155.08	145.56

249

250   **Table 2** Results of ANOVA analysis for current density model

Source	Sum of Squares	DF	Mean Square	F-Value	P-Value Prob>F
Model	20188.97	9	2243.22	24.91	< 0.0001 significant
A: MXene Composition	342.96	1	342.96	3.81	0.0795
B: Nafion Loading	4153.18	1	4153.18	46.13	< 0.0001
C: Methanol Concentration	997.81	1	997.81	11.08	0.0076
A^2	3174.81	1	3174.81	35.26	0.0001
B^2	8729.07	1	8729.07	96.95	< 0.0001
C^2	5452.43	1	5452.43	60.55	< 0.0001
AB	3.30	1	3.30	0.037	0.8520
AC	12.55	1	12.55	0.14	0.7167
BC	8.61	1	8.61	0.096	0.7635
Residual	900.41	10	90.04		
Lack of Fit	637.09	5	127.42	2.42	0.1772 not significant
Pure Error	263.32	5	52.66		
Correlation Total	21089.38	19			

|					
Standard Deviation	9.49		R^2	0.9573	
Mean	141.9		Adj R^2	0.9189	
			Pred R^2	0.7525	
			Adeq R^2	14.746	

251

252   The comparison of changes in the levels of variable combination with changes due to

253   random errors inherent in response measurement is also known as ANOVA analysis (Bezerra

254 et al., 2008). Results generated by RSM provide the F- value, Prob>F and significance of each

255 coefficient for the entire model and presented in Table 2. The higher F-value and lower Prob>F

256 show that the model offers better assurance in explaining the design factor variation of the

257 mean data (Zainoodin et al., 2015). The F-value of 24.91 implies that only 0.01% chance that

258 the model could occur due to noise and the model is significant. The model Prob>F value is

259 <0.0001 which indicate that the model terms are significant. Meanwhile, the lack of fit of 2.42

260 verifies that it is not significant and there is 17.72% chance that it could occur due to the noise.

261 It is a good sign, which indicates the model is fit.

262   The ANOVA also identifies the determination coefficient, R^2 and standard deviation,

263 which can further evaluate the validity of the model. The R^2 and standard deviation of 0.9573

264 and 9.49, implies that 95.73% of the total variation can be corresponded by the model.

265 Furthermore, the 'Pred-R^2' and 'Adj-R^2' values of 0.7525 and 0.9189 are in reasonable

266 agreement. The 'Adeq Precision' value for this model is 14.746, where the value higher than 4

267 are desirable and adequate for this signal to noise ratio measurement. Therefore, the ANOVA

268 indicates that this model can be used to evaluate the experimental data in the design space.

269   The other analysis process for RSM is the diagnostic part. This part will evaluate the

270 model fit and transformation choice with graphs. Fig. 3 shows the model fit error that also

271 called as a residual plot. Normal probability plot of residual in Fig. 3(a) shows that the plots lie

272 on the straight line, meaning that the residual follow the normal distribution and having

273 appropriate normal error terms. Fig. 3(b) is a residual vs predicted value plot of the model

274 response and the graph displaying a straight line at '0', indicating that the predicted variance

275 for this model is constant. At the same time, the proposed quadratic model for the current

276 density model seems adequate and since all the plots are in the region between upper and lower

277 red lines and no unusual pattern is detected.
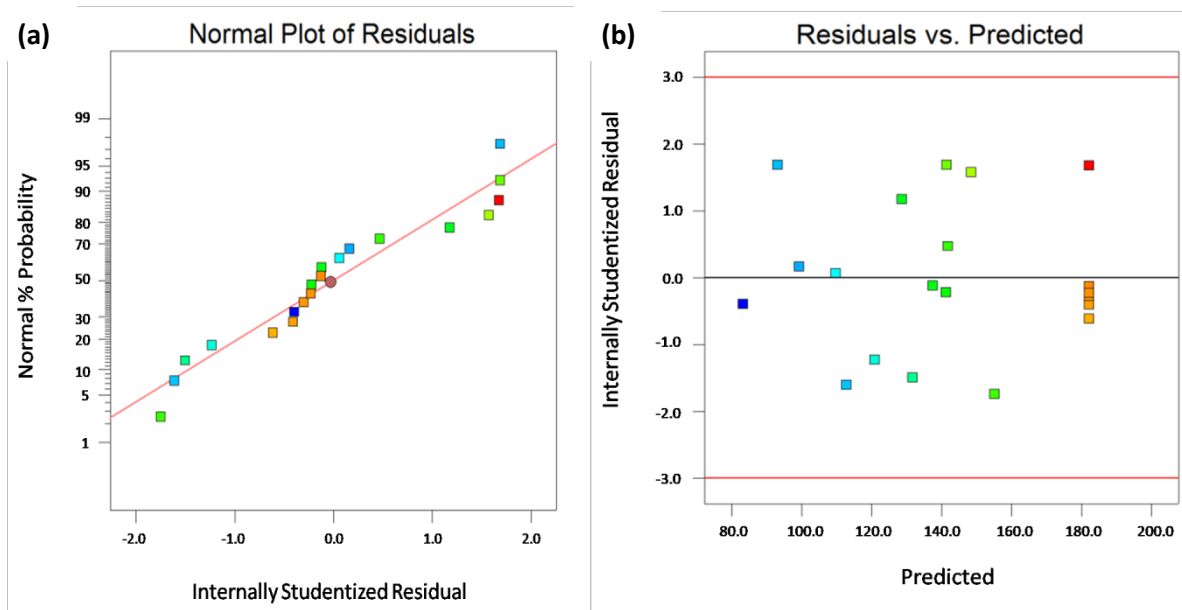
Fig. 3. A residual plot for the current density model; (a) Normal plot of residual, (b) Residual vs predicted plot

The values that are difficult to predict by the model are detected using the predicted vs actual plot (Hasran et al., 2013) and this plot is illustrated in Fig. 4(a). All the plotted data is located along the centre of the graph and make the formation of the perpendicular line with 45° angle. This result reflected the ability of the model to predict the response appropriately. Fig. 4(b) is a perturbation plot, where this plot can show how the factors can give the influence towards the response. As mentioned before, factor A, B and C are MXene composition, Nafion content and methanol concentration, respectively. All the factors are set at the 'coded 0' midpoint with the actual value for all the factors are; A: 77.50wt%, B: 25wt%, C: 2.5M. The perturbation graph is plotted by changing the one factor at one time over the response value. The plot creates the steep slope for all the factors, signify that all three factors show the influenced or sensitivity towards the experimental response and significant to the process model. However, the graph for the factor B show slightly higher in gradient compared to the factor A and C, which suggest the factor B give more effect to the response value.
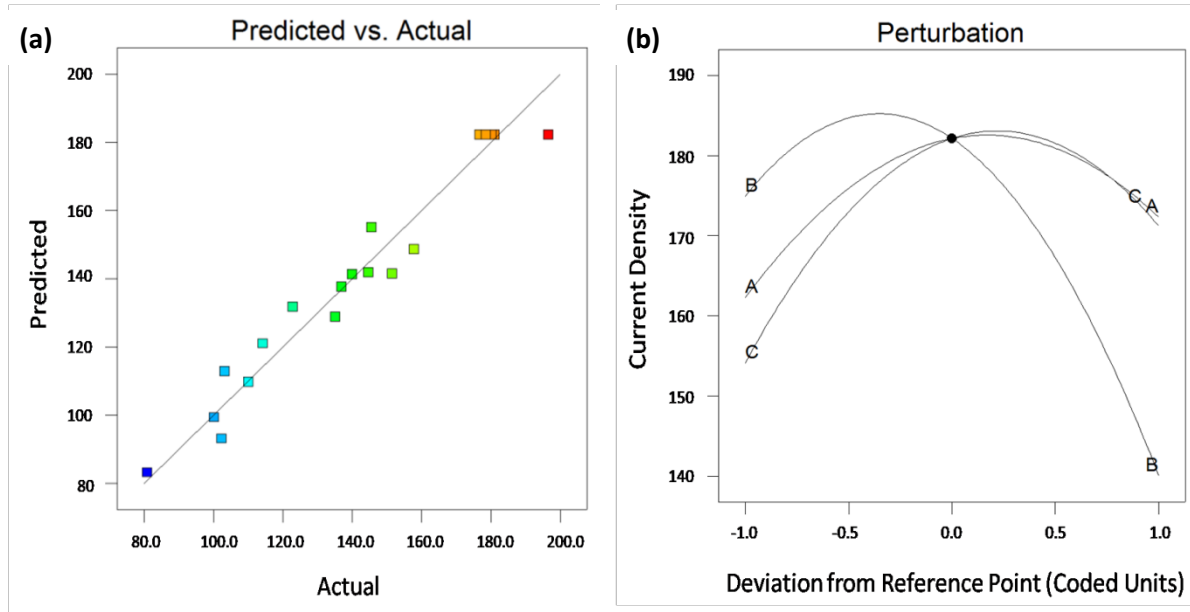
Fig. 4. (a) Predicted vs actual plot and (b) Perturbation plot for the current density model

The response surface analysis involved in predicting the response or estimating the mean response at a particular point in the process factors (Myers et al., 2016). The response surface present in graphical display for 2D contour and three-dimensional (3D) surface plot as illustrated in Fig. 5. The response surface consists of analysis between two factors, namely AB, AC, and BC, with the response of the current density. However, Fig. 5 is an example of an analysis for factors A and B towards current density. The 2D contour plot shows that there is some effect for the interactions between factors A and B and response. The plot reveals that the response is increased when both factors are increased. After achieving some point, the trends of response start to decrease even though the factors value is increasing. This point is called as optimum point, where the optimum factors can contribute the maximum response for the model. The trends for the other factors; AC and BC, towards the responds are almost the same. The optimum point for factors is located at the red area in contour plot, that also known as a high response value area. The 3D surface plot in Fig. 5(b) also illustrated the same trends as in contour plot and the clear peak for all factors is an optimum point that achieved at the maximum response. The factors of AB, AC, and BC exhibit the same trend. The 3D graph

309   pattern corresponds to second-order model by literature (Myers et al., 2016), which proves that

310   quadratic model is fits with current density model.
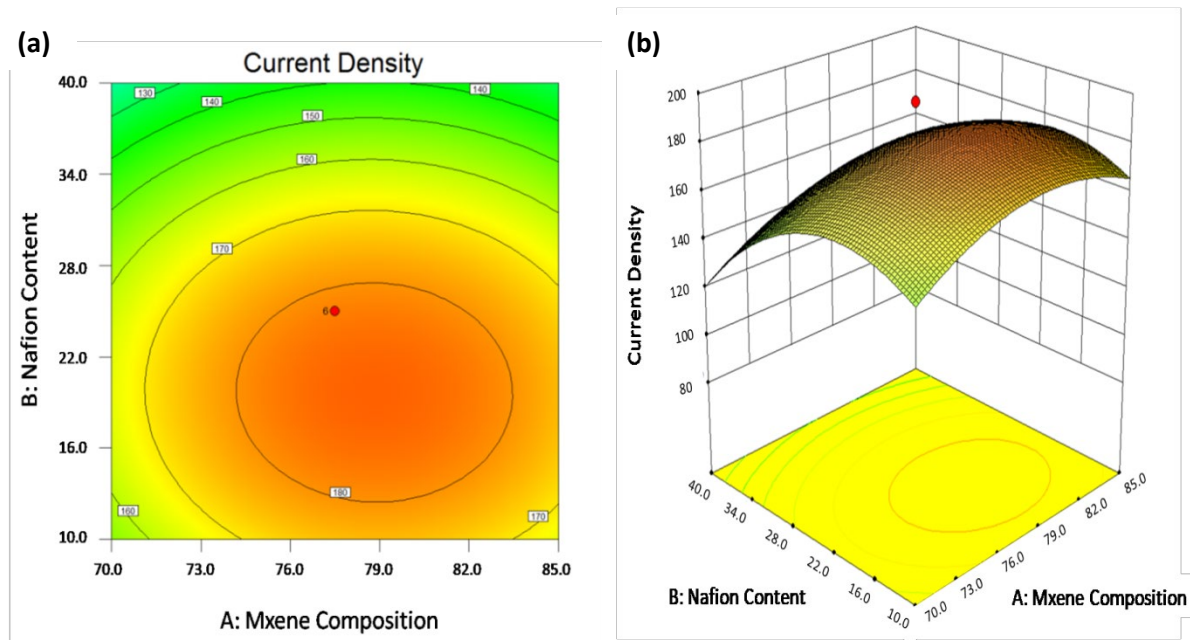
Fig. 5. Response surface between factors; MXene composition and Nafion content, with response; Current density, (a) 2D contour and (b) 3D surface plot

313   The next part in the RSM is the optimization analysis. This part divided into four main

314   categories, numerical optimization, graphical optimization, point prediction and confirmation.

315   The numerical optimization categories involved in setting the goals to predict the optimal

316   conditions factors to generate maximum response as chosen for the goals for this model. Then

317   the graphical optimization takes place and the 2D contour plot for desirability and response

318   prediction value (example for terms of AB factor) are illustrated in Fig. 6(a) and (b). The plot

319   in the high response area extract the prediction value for desirability and response of this model

320   are 0.91 and 186.59mA/mg$_{PtRu}$, respectively. The point prediction for each optimum factor for

321   this model is generated and shown in Fig. 7. The graph shows that all three factors achieve

322   optimal point at the intersection between the graphs with high desirability. The RSM also

323   analyzed the optimum factors value; where A (MXene composition): 78.88wt%, B (Nafion

324   content): 19.71wt%, C (Methanol concentration): 2.82M. Later, validation participates in

comparing the predicted results of the model with the experimental results.
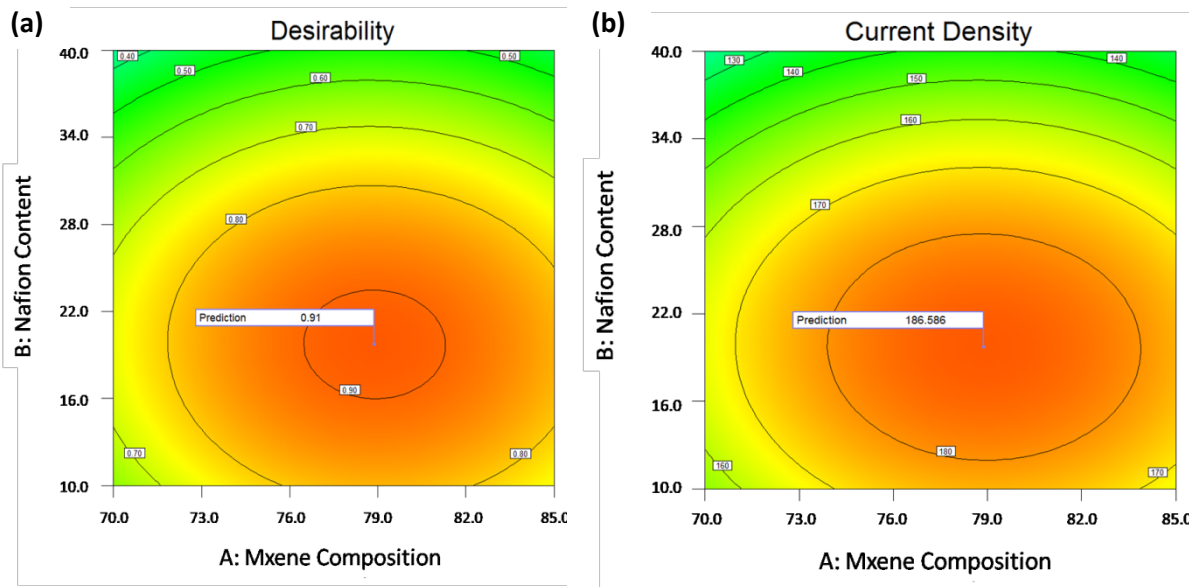
Fig. 6. 2D contour plots for, (a) Desirability and (b) Current density in terms of AB
factors
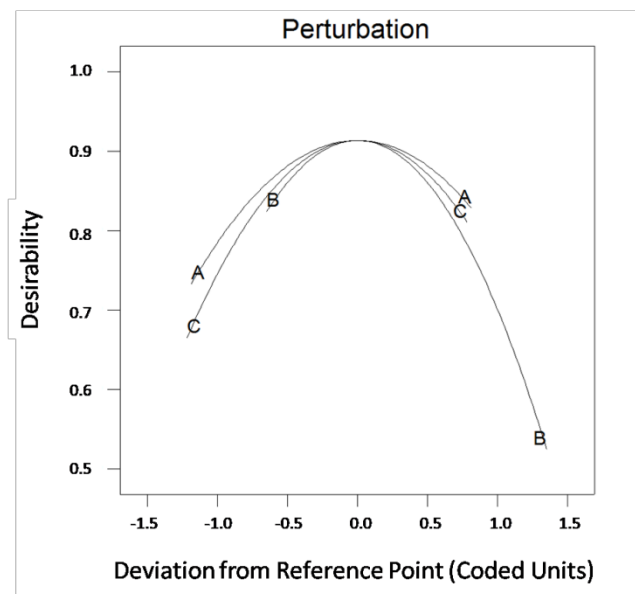
Fig. 7. Perturbation plot for the desirability after optimization analysis

The validation test with the optimal factors value is repeated for three times to get the
average and the result is presented in Table 3. Meanwhile, the current density graph from
validation test is shown in Fig. 8. The response value for this model is extracted from the CV

test that provides electrochemical measurementThe average result for the validation test was 187.05mA/mg$_{PtRu}$ corresponding to the peak potential of 0.66 V vs. Ag/AgClwith only 0.25% error compared to the predicted value by RSM analysis. The small error proves that the optimum MXene composition, Nafion content and methanol concentration can provide the maximum current density response. This scenario also ensures that the model generated by RSM analysis is applicable and successful.
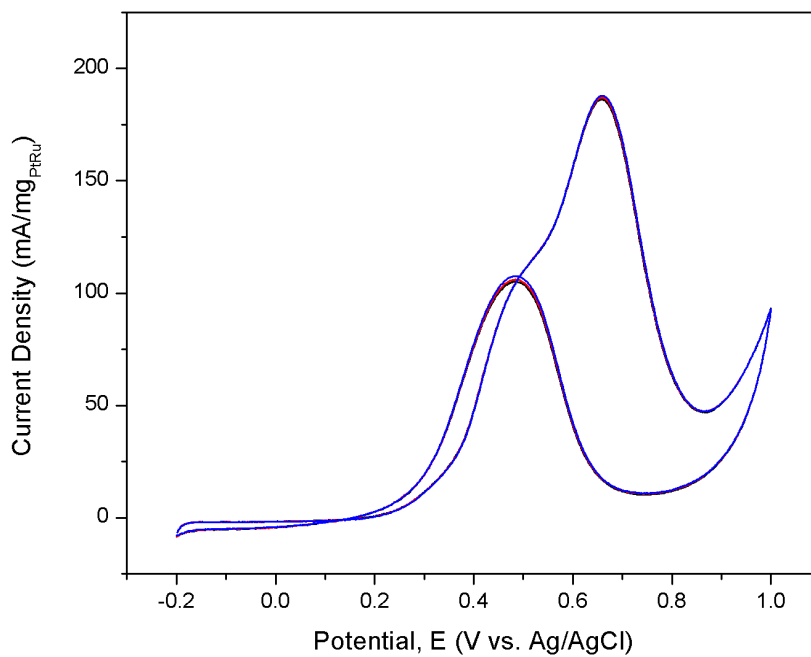
Fig. 8. Validation test for current density model

**Table 3** Validation test results using optimum factors value for current density model

Factor A	Factor B	Factor C	Current Density (mA/mg$_{PtRu}$)					Error
(wt%)	(wt%)	(M)	Prediction	1	2	3	Average	(%)
78.88	19.71	2.82	186.59	186.59	187.13	187.9	187.05	0.25

Fig. 9 shows the comparison between PtRu/MXene electrocatalyst, which is the electrocatalyst for this model, with PtRu/C electrocatalyst; the commercial electrocatalyst for the DMFC application. The results indicate that the current density of PtRu/MXene is 2.34

346 times higher than PtRu/C. This is due unique 2D structures of MXene that can provide fast

347 ion/charge transfer path (Yuan and Cheng, 2019). This unique property is beneficial to surface

348 chemical reaction and helping the electrocatalyst to be more highly active. In addition, the

349 MXene structure as depicted on the surface morphology part, gives an opportunity to Pt and

350 Ru nanoparticles for more attachment to the MXene surface. Therefore, this condition leads to

351 increase the reaction active site with increased electrocatalytic activity of the electrocatalyst.

352 This electrochemical measurement of CV cannot reveal the complete electrocatalyst properties

353 of MXene, and more study need to be done for this material. However, the large differences

354 between these two electrocatalyst indicates that PtRu/MXene have great potential in the field

355 of electrocatalysis especially for fuel cell applications.
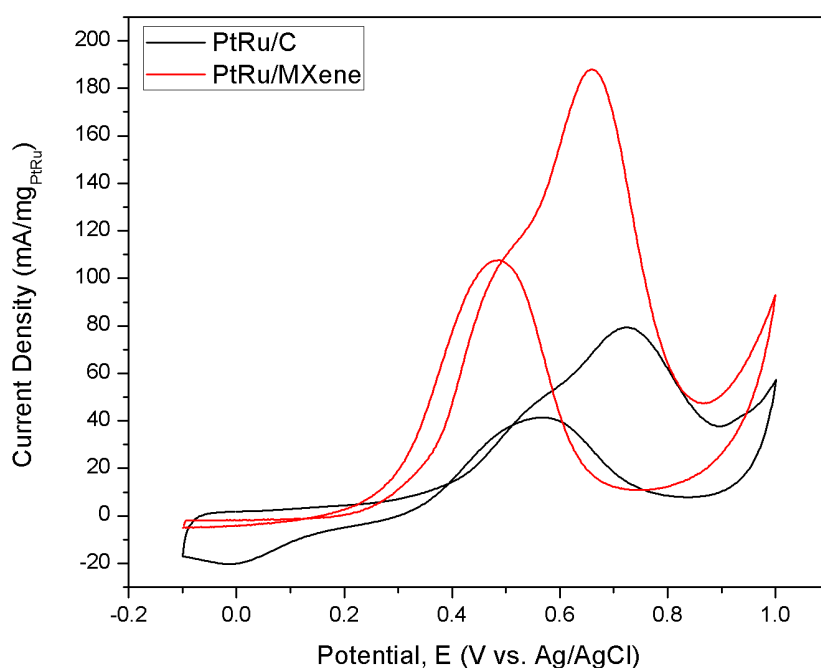
356

357 **Fig. 9.** Comparison of current density from the model with commercial electrocatalyst

358 **Table 4** Comparative table of current density with other literature

Author	Type of Electrocatalyst	Type of Reaction	Current Density (mA/cm^2)

Present study	PtRu/Ti$_3$C$_2$	MOR	12.46
Wang et al. (2019)	Pt/Ti$_3$C$_2$	MOR and HER	1.137
Chen et al. (2019)	Co-CNT/Ti$_3$C$_2$	ORR	5.55
Lin et al. (2019)	Ti$_3$C$_2$	ORR	2.3
Yu et al. (2019)	g-C$_3$N$_4$/Ti$_3$C$_2$	ORR	0.71
Wang et al. (2019)	Pt/C	MOR and HER	0.388
Present study	PtRu/C	MOR	5.283

359

360   The synthesized PtRu/MXene electrocatalyst is compared with other MXene-based

361 electrocatalyst that applied in the electrocatalysis area. The comparison of current density is

362 listed in Table 4 with the unit of current over surface area based on the literature unit.

363 Comparative results show that the peak current density of PtRu/MXene is highest among other

364 electrocatalyst. The high values of current density are aided through combination of bimetallic,

365 Pt and Ru, and MXene. The bimetallic materials are distributed evenly as resulted in mapping

366 analysis, which helps to improve the reaction between these materials. However, the detailed

367 reaction mechanisms between bimetallic and MXene need to be further explored. The high

368 value of PtRu/MXene electrocatalyst is reflected to the high performance for the DMFC

369 technology, which is one of the promising clean energy productions under fuel cell application.

370 This potential seen to be beneficial to wide range of prospect including researcher, industry

371 and world community in track of making the clean energy more firm and commercialized

372 worldwide.

373

374 **4.   CONCLUSIONS**

375 The RSM approach as one of the optimization method for developing and improving the factors

376 that affect the PtRu/MXene electrocatalytic activity has been studied. The factors involved are

377 the MXene composition, Nafion content and methanol concentration; and current density as a

378 response. The generated new quadratic model of current density shows the significant

379 prediction of factors and response. The high response area in 2D contour plot exhibits the

380 response prediction value for this model. The validation test using optimum factors gives the

381 result of current density of 187.05mA/mg$_{PtRu}$, with only 0.25% error with the prediction value

382 (186.59mA/mg$_{PtRu}$). The results indicate that the model generated by RSM was successfully

383 developed with good accuracy. The PtRu/MXene also gives 2.34 times higher current density

384 than PtRu/C . Thus, the new combination between PtRu and 2D materials of MXene show

385 some potential to be one of emerging material in fuel cell application too.

386

387 **ACKNOWLEDGEMENT**

390

391 **REFERENCES**

392 Abdullah, N., Kamarudin, S. K., Shyuan, L. K., Karim, N. A., 2017. Fabrication and

393 characterization of new composite TiO2 carbon nanofiber anodic catalyst support for

394 direct methanol fuel cell via electrospinning method. Nanoscale Research

395 Letters. 12(1), 613.

396 Abdullah, N., Kamarudin, S. K., Shyuan, L. K., 2018. Novel anodic catalyst support for direct

397 methanol fuel cell: characterizations and single-cell performances. Nanoscale Research

398 Letters. 13(1), 90.

399 Abdullah, N., Kamarudin, S. K., Shyuan, L. K., Karim, N. A., 2019. Synthesis and optimization

400 of PtRu/TiO2-CNF anodic catalyst for direct methanol fuel cell. International Journal

401 of Hydrogen Energy. 44(58), 30543-30552.

402   Adilbish, G., Yu, Y. -T., 2017. Effect of the Nafion content in the MPL on the catalytic activity

403   of the Pt/C-Nafion electrode prepared by pulsed electrophoresis deposition.

404   International Journal of Hydrogen Energy. 42(2), 1181-1188.

405   Asfaram, A., Ghaedi, M., Agarwal, S., Tyagi, I., Gupta, V. K., 2015. Removal of basic dye

406   Auramine-O by ZnS: Cu nanoparticles loaded on activated carbon: optimization of

407   parameters using response surface methodology with central composite design. RSC

408   Advances. 5(24), 18438-18450.

409   Aslfattahi, N., Saidur, R., Arifutzzaman, A., Sadri, R., Bimbo, N., Sabri, M. F. M., Maughan,

410   P. A., Bouscarrat, L., Dawson, R. J., Said, S. M., Goh, B. T., 2020. Experimental

411   investigation of energy storage properties and thermal conductivity of a novel organic

412   phase change material/MXene as a new class of nanocomposites. Journal of Energy

413   Storage. 27, 101115.

414   Bezerra, M. A., Santelli, R. E., Oliveira, E. P., Villar, L. S., Escaleira, L. A., 2008. Response

415   surface methodology (RSM) as a tool for optimization in analytical chemistry. Talanta.

416   76(5), 965-977.

417   Caponi, N., Collazzo, G. C., Salla, J. D. S., Jahn, S. L., Dotto, G. L., Foletto, E. L., 2019.

418   Optimisation of crystal violet removal onto raw kaolin using response surface

419   methodology. International Journal of Environmental Technology and Management.

420   22(2-3), 85-100.

421   Chen, J., Yuan, X., Lyu, F., Zhong, Q., Hu, H., Pan, Q., Zhang, Q., 2019. Integrating MXene

422   nanosheets with cobalt-tipped carbon nanotubes for an efficient oxygen reduction

423   reaction. Journal of Materials Chemistry A. 7(3), 1281-1286.

424   Chia, X., Pumera, M., 2018. Characteristics and performance of two-dimensional materials

425   for electrocatalysis. Nature Catalysis. 1.

426 Danmaliki, G. I., Saleh, T. A., Shamsuddeen, A. A., 2017. Response surface methodology
427   optimization of adsorptive desulfurization on nickel/activated carbon. Chemical
428   Engineering Journal. 313, 993-1003.

429 Dharma, S., Masjuki, H. H., Ong, H. C., Sebayang, A. H., Silitonga, A. S., Kusumo, F., Mahlia,
430   T. M. I., 2016. Optimization of biodiesel production process for mixed Jatropha curcas–
431   Ceiba pentandra biodiesel using response surface methodology. Energy Conversion and
432   Management. 115, 178-190.

433 Deivaraj, T., Lee, J. Y., 2005. Preparation of carbon-supported PtRu nanoparticles for direct
434   methanol fuel cell applications–a comparative study. Journal of Power Sources. 142(1-
435   2), 43-49.

436 Fletcher, R., 2013. Practical methods of optimization. John Wiley & Sons.

437 Han, J., Yang, L., Yang, L., Jiang, W., Luo, X., Luo, S., 2018. PtRu nanoalloys loaded on
438   graphene and TiO2 nanotubes co-modified Ti wire as an active and stable methanol
439   oxidation electrocatalyst. International Journal of Hydrogen Energy. 43(15), 7338-
440   7346.

441 Hasran, U. A., Kamarudin, S. K., Daud, W. R. W., Majlis, B. Y., Mohamad, A. B., Kadhum,
442   A. A. H., Ahmad, M. M., 2013. Optimization of hot pressing parameters in membrane
443   electrode assembly fabrication by response surface method. International Journal of
444   Hydrogen Energy. 38(22), 9484-9493.

445 Ito, Y., Takeuchi, T., Tsujiguchi, T., Abdelkareem, M. A., Nakagawa, N., 2013. Ultrahigh
446   methanol electro-oxidation activity of PtRu nanoparticles prepared on TiO2-embedded
447   carbon nanofiber support. Journal of Power Sources. 242, 280-288.

448 Joghee, P., Malik, J. N., Pylypenko, S., O'Hayre, R., 2015. A review on direct methanol fuel
449   cells–in the perspective of energy and sustainability. MRS Energy & Sustainability. 2.

450   Karim, N. A., Yahya, N., 2018. A short overview current research of catalyst for methanol
451   oxidation reaction in direct methanol fuel cell (DMFC) from experimental and
452   theoretical aspect. Jurnal Kejuruteraan. 1(2), 9-17.

453   Khatti, T., Naderi-Manesh, H., Kalantar, S. M., 2019. Application of ANN and RSM
454   techniques for modeling electrospinning process of polycaprolactone. Neural
455   Computing and Applications. 31(1), 239-248.

456   Khazaei, M., Mishra, A., Venkataramanan, N. S., Singh, A. K., Yunoki, S., 2019. Recent
457   advances in MXenes: from fundamentals to applications. Current Opinion in Solid
458   State and Materials Science.

459   Kivrak, H. D., 2015. The effect of temperature and concentration for methanol electrooxidation
460   on Pt-Ru catalyst synthesized by microwave assisted route. Turkish Journal of
461   Chemistry. 39(3), 563-575.

462   Kuang, P., He, M., Zhu, B., Yu, J., Fan, K., Jaroniec, M., 2019. 0D/2D NiS2/V-MXene
463   composite for electrocatalytic H2 evolution. Journal of Catalysis. 375, 8-20.

464   Lei, J. C., Zhang, X., Zhou, Z., 2015. Recent advances in MXene: preparation, properties,
465   and applications. Frontiers of Physics. 10(3), 276-286.

466   Lin, H., Chen, L., Lu, X., Yao, H., Chen, Y., Shi, J., 2019. Two-dimensional titanium carbide
467   MXenes as efficient non-noble metal electrocatalysts for oxygen reduction reaction.
468   Science China Materials. 62(5), 662-670.

469   Luo, F., Zhang, Q., Qu, K., Guo, L., Hu, H., Yang, Z., Cai, W., Cheng, H., 2019. Decorated
470   PtRu electrocatalyst for concentrated direct methanol fuel cells. ChemCatChem. 11(4),
471   1238-1243.

472   Masdar, M. S., Puaad, N. A., Aslam, N. M., Kamarudin, S. K., 2016. Effect of teflon and nafion
473   loading at anode in direct formic acid fuel cell (DFAFC). Journal of Engineering
474   Science and Technology. 11(8), 1121-1134.

475 Myers, R. H., Montgomery, D. C., Anderson-Cook, C. M., 2016. Response surface methodology: process and product optimization using designed experiments. John Wiley & Sons.

478 Park, J. C., Choi, C. H., 2017. Graphene-derived Fe/Co-NC catalyst in direct methanol fuel cells: Effects of the methanol concentration and ionomer content on cell performance. Journal of Power Sources. 358, 76-84.

481 Shaari, N., Kamarudin, S. K., 2018. Performance of crosslinked sodium alginate/sulfonated graphene oxide as polymer electrolyte membrane in DMFC application: RSM optimization approach. International Journal of Hydrogen Energy. 43(51), 22986-23003.

485 Stone, C., 2007. Fuel cell technologies powering portable electronic devices. Fuel Cells Bulletin. 2007(10), 12-15.

487 Sulaiman, N. S., Hashim, R., Amini, M. H. M., Danish, M., Sulaiman, O., 2018. Optimization of activated carbon preparation from cassava stem using response surface methodology on surface area and yield. Journal of Cleaner Production. 198, 1422-1430.

490 Tran, M. H., Schäfer, T., Shahraei, A., Dürrschnabel, M., Molina-Luna, L., Kramm, U. I., Birkel, C. S., 2018. Adding a new member to the MXene family: synthesis, structure, and electrocatalytic activity for the hydrogen evolution reaction of V4C3T x. ACS Applied Energy Materials. 1(8), 3908-3914.

494 Vecchio, C. L., Sebastián, D., Alegre, C., Aricò, A. S., Baglio, V., 2018. Carbon-supported Pd and Pd-Co cathode catalysts for direct methanol fuel cells (DMFCs) operating with high methanol concentration. Journal of Electroanalytical Chemistry. 808, 464-473.

497 Wang, Y., Wang, J., Han, G., Du, C., Deng, Q., Gao, Y., Yin, G., Song, Y., 2019. Pt decorated Ti3C2 MXene for enhanced methanol oxidation reaction. Ceramics International. 45(2), 2411-2417.

Xia, Z., Huang,Q., Guo,S., 2019. Recent progress on synthesis, structure and electrocatalytic applications of MXenes. FlatChem. 100129.

Xie, X., Chen, S., Ding, W., Nie, Y., Wei, Z., 2013. An extraordinarily stable catalyst: Pt NPs supported on two-dimensional $Ti_3C_2X_2$ (X= OH, F) nanosheets for oxygen reduction reaction. Chemical Communications. 49(86), 10112-10114.

Yahya, N., Kamarudin, S. K., Karim, N. A., Masdar, M. S., Loh, K. S., 2017. Enhanced performance of a novel anodic PdAu/VGCNF catalyst for electro-oxidation in a glycerol fuel cell. Nanoscale Research Letters. 12(1), 605.

Yang, X., Jia, Q., Duan, F., Hu, B., Wang, M., He, L., Song, Y., Zhang, Z., 2019. Multiwall carbon nanotubes loaded with MoS_2 quantum dots and MXene quantum dots: non–Pt bifunctional catalyst for the methanol oxidation and oxygen reduction reactions in alkaline solution. Applied Surface Science. 464, 78-87.

Yu, X., Yin, W., Wang, T., Zhang, Y.,2019. Decorating g-C3N4 nanosheets with Ti3C2 MXene nanoparticles for efficient oxygen reduction reaction. Langmuir. 35(8), 2909-2916.

Yuan, W., Cheng, L., 2019. MXenes for electrocatalysis. MXenes: Fundamentals and Applications. 51, 74-104.

Zainoodin, A. M., Kamarudin, S. K., Masdar, M. S., Daud, W. R. W., Mohamad, A. B., Sahari, J., 2015. Optimization of a porous carbon nanofiber layer for the membrane electrode assembly in DMFC. Energy Conversion and Management. 101, 525-531.

Zhang, Q., Yang, Z., Yang, J., Yu, X., Ling, Y., Zhang, Y., Cai, W., Cheng, H., 2018. Carbon nitride simultaneously boosted a PtRu electrocatalyst's stability and electrocatalytic activity toward concentrated methanol. Chemical Communications, 54(67), 9282-9285.

524   Zhang, X., Zhang, J., Cao, H., Li, Y., 2019. Preparation of Pt/(Ti3C2Tx) y-(MWCNTs) 1-y

525   electrocatalysts via a facile and scalable solvothermal strategy for high-efficiency

526   methanol oxidation. Applied Catalysis A: General. 585, 117181.

527   Zhang, Z., Li, H., Zou, G., Fernandez, C., Liu, B., Zhang, Q., Hu, J., Peng, Q., 2016. Self-

528   reduction synthesis of new MXene/Ag composites with unexpected electrocatalytic

529   activity. ACS Sustainable Chemistry & Engineering. 4(12), 6763-6771.

530   Zhu, J., Ha, E., Zhao, G., Zhou, Y., Huang, D., Yue, G., Hu, L., Sun, N., Wang, Y., Lee, L.Y.,

531   Xu, C., 2017. Recent advance in MXenes: a promising 2D material for catalysis, sensor

532   and chemical adsorption. Coordination Chemistry Reviews. 352, 306-327.